Cellular/Molecular

Developmental Expression of Ca^{2+}-Permeable AMPA Receptors Underlies Depolarization-Induced Long-Term Depression at Mossy Fiber–CA3 Pyramid Synapses

Michelle T.-W. Ho,[1,3] Kenneth A. Pelkey,[1] Lisa Topolnik,[4] Ronald S. Petralia,[2] Kogo Takamiya,[5] Jun Xia,[5] Richard L. Huganir,[5] Jean-Claude Lacaille,[4] and Chris J. McBain[1]

[1]National Institute of Child Health and Human Development and [2]National Institute on Deafness and Other Communication Disorders, National Institutes of Health, Bethesda, Maryland 20892, [3]Department of Biochemistry, The Chinese University of Hong Kong, Hong Kong, The People's Republic of China, [4]Département de Physiologie, Groupe de Recherche sur le Système Nerveux Central, Université de Montréal, Montréal, Québec, Canada H3C 3J7, and [5]Department of Neuroscience, Johns Hopkins University, Baltimore, Maryland 21205

Many central excitatory synapses undergo developmental alterations in the molecular and biophysical characteristics of postsynaptic ionotropic glutamate receptors via changes in subunit composition. Concerning AMPA receptors (AMPARs), glutamate receptor 2 subunit (GluR2)-containing, Ca^{2+}-impermeable AMPARs (CI-AMPARs) prevail at synapses between mature principal neurons; however, accumulating evidence indicates that GluR2-lacking, Ca^{2+}-permeable AMPARs (CP-AMPARs) contribute at these synapses early in development. Here, we used a combination of imaging and electrophysiological recording techniques to investigate potential roles for CP-AMPARs at developing hippocampal mossy fiber–CA3 pyramidal cell (MF–PYR) synapses. We found that transmission at nascent MF–PYR synapses is mediated by a mixed population of CP- and CI-AMPARs as evidenced by polyamine-dependent inwardly rectifying current–voltage (*I–V*) relationships, and partial philanthotoxin sensitivity of synaptic events. CP-AMPAR expression at MF–PYR synapses is transient, being limited to the first 3 postnatal weeks. Moreover, the expression of CP-AMPARs is regulated by the PDZ (postsynaptic density-95/Discs large/zona occludens-1) domain-containing protein interacting with C kinase 1 (PICK1), because MF–PYR synapses in young PICK1 knock-out mice are philanthotoxin insensitive with linear *I–V* relationships. Strikingly, MF–PYR transmission via CP-AMPARs is selectively depressed during depolarization-induced long-term depression (DiLTD), a postsynaptic form of MF–PYR plasticity observed only at young MF–PYR synapses. The selective depression of CP-AMPARs during DiLTD was evident as a loss of postsynaptic CP-AMPAR-mediated Ca^{2+} transients in PYR spines and reduced rectification of MF–PYR synaptic currents. Preferential targeting of CP-AMPARs during DiLTD is further supported by a lack of DiLTD in young PICK1 knock-out mice. Together, these findings indicate that the transient participation of CP-AMPARs at young MF–PYR synapses dictates the developmental window to observe DiLTD.

Key words: **LTD; GluR2; mossy fiber; hippocampus; synapse development; calcium**

Introduction

The glutamate receptor 2 (GluR2) subunit dictates several AMPAR biophysical properties and interacts with various molecules implicated in receptor trafficking (Dingledine et al., 1999; Collingridge et al., 2004; Isaac et al., 2007). Typically GluR2 mRNA undergoes efficient editing at the "Q/R site" (Hollmann et al., 1991; Sommer et al., 1991; Verdoorn et al., 1991; Burnashev et al., 1992; Seeburg et al., 1998), and incorporation of these edited subunits into AMPARs results in low-conductance, Ca^{2+}-impermeable channels (CI-AMPARs) with relatively linear *I–V* relationships. In contrast, AMPARs lacking edited GluR2 have higher conductance, are readily Ca^{2+} permeable (CP-AMPARs), and exhibit inwardly rectifying *I–V* relationships caused by voltage-dependent channel block by intracellular polyamines (Bowie and Mayer, 1995; Donevan and Rogawski, 1995; Kamboj et al., 1995; Koh et al., 1995). Thus, the presence or absence of GluR2 greatly influences AMPAR and, hence, synaptic function.

The ubiquitous expression and efficient editing of GluR2 within principal neurons ensures that CI-AMPARs dominate transmission between excitatory neurons throughout the ner-

Received June 12, 2007; revised Aug. 28, 2007; accepted Sept. 3, 2007.

This research was supported by National Institutes of Health (NIH) intramural awards [National Institute of Child Health and Human Development (C.J.M.) and National Institute on Deafness and Other Communication Disorders (R.S.P.)], NIH extramural and Howard Hughes Medical Institute awards (R.L.H.), as well as Canada Research Chairs, Canadian Institutes of Health Research (CIHR), and Fonds de la Recherche en Santé du Québec awards (J.-C.L.). K.A.P. is an NIH Visiting Fellow and a CIHR Fellow. L.T. received support from the Savoy Foundation. We thank Xiaoqing Yuan, Brian Jeffries, and Dr. Ya-Xian Wang for expert technical assistance.

Correspondence should be addressed to Kenneth A. Pelkey, Laboratory on Cellular and Synaptic Neurophysiology, Building 35, Room 3C705, National Institute of Child Health and Human Development, Bethesda, MD 20892. E-mail: pelkeyk2@mail.nih.gov.

L. Topolnik's present address: Department of Biochemistry and Microbiology, Université Laval, Québec, Québec, Canada G1J 2GS.

J. Xia's present address: Department of Biochemistry, Hong Kong University of Science and Technology, Kowloon, Hong Kong, The People's Republic of China.

DOI:10.1523/JNEUROSCI.2671-07.2007

 0270-6474/07/2711651-12$15.00/0

vous system. However, recent findings indicate GluR2-lacking, CP-AMPARs are assembled in principal neurons and become synaptically incorporated under certain conditions (Aizenman et al., 2002; Kumar et al., 2002; Eybalin et al., 2004; Ju et al., 2004; Terashima et al., 2004; Bagal et al., 2005; Harms et al., 2005; Ogoshi et al., 2005; Shin et al., 2005; Thiagarajan et al., 2005; Clem and Barth, 2006; Plant et al., 2006; Sutton et al., 2006). One compelling line of evidence suggests that CP-AMPARs are transiently expressed by principal neurons early in development. For example, synaptic CP-AMPARs occur in layer 5 pyramids until postnatal day 16 after which CI-AMPARs dominate transmission (Kumar et al., 2002). Similar developmental switches happen at inner hair cell synapses (Eybalin et al., 2004), *Xenopus* retinotectal synapses (Aizenman et al., 2002), and chicken forebrain synapses (Migues et al., 2007). Moreover, developmental increases in the ratio of GluR2 to other AMPAR subunits occur throughout the CNS (Pellegrini-Giampietro et al., 1992; Pickard et al., 2000; Zhu et al., 2000). Such transient CP-AMPAR expression could provide a potentially important route for Ca^{2+} entry during synapse maturation and impart distinct short/long-term plastic properties to developing networks (Rozov and Burnashev, 1999; Liu and Cull-Candy, 2000).

In the hippocampus, mossy fiber–CA3 pyramidal cell (MF–PYR) connections mature entirely postnatally providing an attractive model to probe for AMPAR changes during synapse development in a defined central pathway (Amaral and Dent, 1981; Henze et al., 2000). Moreover, MF–PYR synapses constitutively insert overexpressed GluR1 homomers in contrast to synapses between PYRs in which such recombinant CP-AMPARs are excluded unless driven by CaMKII (calcium/calmodulin-dependent protein kinase II) (Kakegawa et al., 2004), suggesting that MF–PYR synapses are inherently permissive sites for CP-AMPARs. Hence, in the current study we investigated whether native CP-AMPARs contribute to basal transmission and synaptic plasticity at developing MF–PYR synapses.

Materials and Methods

Hippocampal slice preparation. Slices were prepared as described previously (Pelkey et al., 2005; Topolnik et al., 2005) using postnatal day 10 (P10) to P30 Sprague Dawley rats or C57BL/6 mice as indicated throughout the paper, except for experiments involving transgenic animals, which were created on a hybrid genetic background of 129 and C57BL/6 strains (Gardner et al., 2005). Briefly, animals were anesthetized with isoflurane and decapitated allowing removal of the brain into ice-cold saline solution containing the following (in mM): 130 NaCl, 24 $NaHCO_3$, 3.5 KCl, 1.25 NaH_2PO_4, 0.5 $CaCl_2$, 5.0 $MgCl_2$ (or $MgSO_4$), and 10 glucose, saturated with 95% O_2 and 5% CO_2, pH 7.4. In some cases, NaCl was substituted with sucrose (250 mM). After dissection of the brain, individual hemispheres were transferred to the stage of a VT-1000S vibratome (Leica Microsystems, Bannockburn, IL) and sectioned to yield transverse hippocampal slices (300 μm), which were incubated in the above solution at 35°C for recovery until use (minimum 1 h recovery). All animal procedures conformed to the National Institutes of Health and Université de Montréal animal welfare guidelines.

Whole-cell recordings. Individual slices were transferred to a recording chamber and perfused (2–3 ml/min) with extracellular solution composed of the following (in mM): 130 NaCl, 24 $NaHCO_3$, 3.5 KCl, 1.25 NaH_2PO_4, 2.5 $CaCl_2$, 1.5 $MgCl_2$ (or $MgSO_4$), 10 glucose, 0.0025 bicuculline methobromide, and 0.05–0.100 DL-AP5, saturated with 95% O_2 and 5% CO_2, pH 7.4, 32–35°C. Whole-cell patch-clamp recordings using multiclamp 700A or Axopatch 200B amplifiers (Molecular Devices, Foster City, CA) in voltage-clamp mode (V_h, −60 mV) were made from individual CA3 pyramidal neurons, visually identified with infrared video microscopy and differential interference contrast optics. For Ca^{2+} imaging recordings, electrodes (4–5 MΩ) pulled from borosilicate glass (World Precision Instruments, Sarasota, FL) were filled with intracellular solution (ICS) composed of the following (in mM): 130 $CsMeSO_3$, 5 CsCl, 2 $MgCl_2$, 5 diNa-phosphocreatine, 10 HEPES, 2 ATP_2Na, 0.4 GTPNa, 0.1 spermine, 1 lidocaine *N*-ethyl bromide (QX314), and 0.05 OGB1 (Oregon Green 488 BAPTA-1, hexapotassium salt) (Invitrogen, Eugene, OR), pH 7.2–7.3, 275–285 mOsm. For all other recordings, electrodes were filled with ICS of the following composition (in mM): 100 Cs-gluconate, 5 CsCl, 0.6 EGTA, 5 $MgCl_2$, 8 NaCl, 2 Na_2ATP, 0.3 NaGTP, 40 HEPES, 1 QX314, and 0.1 spermine, pH 7.2–7.3 and 290–300 mOsm. In experiments in which reagents were delivered postsynaptically through the recording pipette, we waited a minimum of 15 min after establishing the whole-cell configuration before any attempt was made to induce plasticity to ensure adequate diffusion of reagents into proximal dendritic compartments. The generation of the EVKI (KKEGYNVYGIEEVKI) and SGKA (KKEGYNVYGIESGKA) peptides has been described previously (Gardner et al., 2005). These peptides (200 μM) were applied together with a peptidase inhibitor mixture containing leupeptin, bestatin, and pepstatin (all at 0.1 mM) to prevent degradation. The EVKI peptide serves as a GluR2 c-tail phosphomimic and selectively disrupts GluR2–protein interacting with C kinase 1 (PICK1) postsynaptic density-95/Discs large/zona occludens-1 (PDZ) domain-mediated interactions, and the SGKA peptide is a GluR2 c-tail mutant peptide that does not function as a PDZ binding motif. Data were not corrected for liquid junction potentials. Uncompensated series resistance (8–15 MΩ) was rigorously monitored by the delivery of small voltage steps at regular intervals, and recordings were discontinued after changes of >15%.

Synaptic responses were typically evoked at 0.33 Hz by low-intensity microstimulation (100 μs duration; 20–40 μA intensity) via a constant-current isolation unit (A360; World Precision Instruments, Sarasota, FL) connected to a patch electrode filled with oxygenated extracellular solution. For MF–PYR synaptic recordings, the stimulating electrode was placed in either the dentate gyrus or stratum lucidum. Except in Ca^{2+} imaging recordings, MF origin of EPSCs was always confirmed by perfusion of slices with the group II metabotropic glutamate receptor (mGluR) agonist 2*S*,2′*R*,3′*R*-2-(2′,3′-dicarboxy-cyclopropyl)glycine (DCGIV) (1 μM) (Kamiya et al., 1996). For PYR collateral fiber stimulation, the stimulating electrode was placed in CA3 stratum radiatum and evoked events did not exhibit DCGIV sensitivity. MF–PYR depolarization-induced long-term depression (DiLTD) was induced by depolarizing the postsynaptic CA3 pyramidal cell from −60 to −10 mV for 5 min in the absence of stimulation (Lei et al., 2003). Data for *I–V* curves were obtained by varying the postsynaptic membrane potential between −60 and +40 mV in steps of 20 mV.

Data analysis. For each recording, EPSC amplitudes from individual sweeps were measured during a 1–2 ms window around the peak of the waveform. Then, for incorporation into group data, the EPSC amplitudes for a given recording were binned as consecutive 1 min averages and normalized to the mean amplitude obtained during the baseline period (first 3–10 min). Data are presented as means ± SEMs unless otherwise indicated. Statistical significance was assessed using both parametric (paired and unpaired *t* tests) and nonparametric (Mann–Whitney or Wilcoxon signed-rank tests) statistical analyses as appropriate. Unless otherwise indicated, *p* values reported throughout the manuscript correspond to values obtained using nonparametric analyses. For some recordings, paired-pulse ratios (PPRs) were obtained by calculating mean P2/mean P1, where P1 represents the amplitude of the first evoked current and P2 the amplitude of the second for 20 consecutive individual traces. For *I–V* relationships, a minimum of five events was averaged for each holding potential. To determine rectification indexes (RIs), the negative portion of individual *I–V* relationships (between V_h of −60 and 0 mV) was fit by a linear regression, and then RI was calculated as the ratio of the actual current amplitude observed at +40 mV to the predicted value at +40 mV based on the linear regression. Alternatively, in experiments in which the RI was monitored before and after DiLTD, RI was determined as the absolute value of the ratio of the mean current amplitude at +40 mV to the mean current amplitude at −60 mV ($RI_{EPSC+40/EPSC-60}$).

Ca^{2+} imaging of thorny excrescences. After obtaining the whole-cell configuration, 20–30 min were allowed for intracellular diffusion of the

fluorophore. Imaging was performed using a two-photon laser scanning microscope LSM 510 (Carl Zeiss, Kirkland, Quebec, Canada) based on a mode-locked Ti:sapphire laser operating at 800 nm, 76 MHz pulse repeat, <200 fs pulse width, and pumped by a solid-state source (Mira 900 and 5 W Verdi argon ion laser; Coherent, Santa Clara, CA). A long-range water-immersion objective (40×; numerical aperture, 0.8) was used. Fluorescence was detected through a short-pass filter (cutoff, 680 nm) in non-descanned detection mode and images were acquired using the LSM 510 software (Carl Zeiss). Ca^{2+} transients (average of four responses) evoked by local electrical stimulation were measured at 20–40 μm from the soma by scanning a line through the thorny excrescence. Changes in fluorescence were calculated relative to the baseline and expressed as $\%\Delta F/F = [(F - F_{rest})/F_{rest}] \times 100$. Summary data are expressed as mean ± SE.

Immunogold electron microscopy. Immunogold studies were done as described previously (Petralia and Wenthold, 1999; Petralia et al., 1999; Rouach et al., 2005). Briefly, mice were perfused with 4% paraformaldehyde plus 0.5% glutaraldehyde and sections were frozen in liquid propane in a Leica CPC and freeze-substituted into Lowicryl HM-20 in a Leica AFS. Ultrathin sections were incubated in 0.1% sodium borohydride plus 50 mM glycine in Tris-buffered saline plus 0.1% Triton X-100 (TBST), and then in 10% normal goat serum (NGS) in TBST, and then in primary antibody in 1% NGS/TBST, followed by immunogold in 1% NGS/TBST/0.5% polyethylene glycol (molecular weight, 20,000), and then stained with uranyl acetate and lead citrate. Figures were processed with Adobe Photoshop with minimal use of levels, brightness, and contrast used uniformly over the images. Double immunogold labeling used a rabbit polyclonal antibody to GluR1 (Petralia and Wenthold, 1992) with 5 nm immunogold, and a mouse monoclonal antibody to GluR2 (Steinberg et al., 2006) with 15 nm immunogold. Control sections where primary antibodies were omitted did not produce significant 5 and 15 nm gold labeling. Micrographs were taken in the CA3 stratum lucidum at 20,000× for identification of mossy terminal/spine associations and at 40,000× for quantitative analysis. Mossy fiber terminals were identified as large, irregular structures with many round synaptic vesicles contacting complex spines (thorny excrescences) originating from CA3 pyramidal cell apical dendrites. Identification and characterization of these structures have been described in great detail (Petralia and Wenthold, 1992; Darstein et al., 2003). Gold particles in both the synaptic cleft and postsynaptic density were considered membrane associated and synaptic. At extrasynaptic sites of spine profile membranes, only gold particles within 20 nm of the membrane were considered membrane associated [based on the resolution of the immunogold method (Rouach et al., 2005)]. We examined total surface labeling by combining the synaptic and extrasynaptic counts on each spine profile. Then, for each spine profile, we compared synapses in which 5 nm gold labeling for GluR1 was >100 nm from any 15 nm gold particle ("5 nm only") to those in which 5 and 15 nm gold particles were <100 nm apart ("5 + 15 nm"). The former group was intended to represent synaptic AMPA receptors that were more likely to lack GluR2 than the latter group; 100 nm was selected arbitrarily for the sake of comparison between the wild-type and mutant mice. Immunogold labeling is expected only to represent some fraction of total receptor labeling (Petralia et al., 1999).

Results

Transient expression of CP-AMPARs at developing MF–PYR synapses

AMPARs lacking edited GluR2 subunits exhibit pronounced inward rectification caused by voltage-dependent block of the channel pore by intracellular polyamines, providing a convenient electrophysiological signature to assess the contribution of CP-AMPARs to synaptic transmission (Bowie and Mayer, 1995; Donevan and Rogawski, 1995; Kamboj et al., 1995; Koh et al., 1995). Thus, to initially probe for the presence of CP-AMPARs at developing MF–PYR synapses, we examined *I–V* relationships of pharmacologically isolated (50–100 μM DL-APV) AMPAR-mediated MF–PYR EPSCs in slices from young (P10–P17) mice. At this stage of development, using an intracellular recording solution (ICS) supplemented with the polyamine spermine (100 μM), we consistently observed significant rectification in MF–PYR EPSC *I–V* relationships (Fig. 1*A*, top panel). The degree of rectification for each recording was quantified by calculating the ratio of the actual EPSC value observed at a holding potential (V_h) of +40 mV to that predicted by a linear fit of the *I–V* relationship at holding potentials between −60 and 0 mV (see Materials and Methods). For MF–PYR synapses in slices obtained from P10–P17 mice, this RI ranged from 0.12 to 0.69 (mean ±

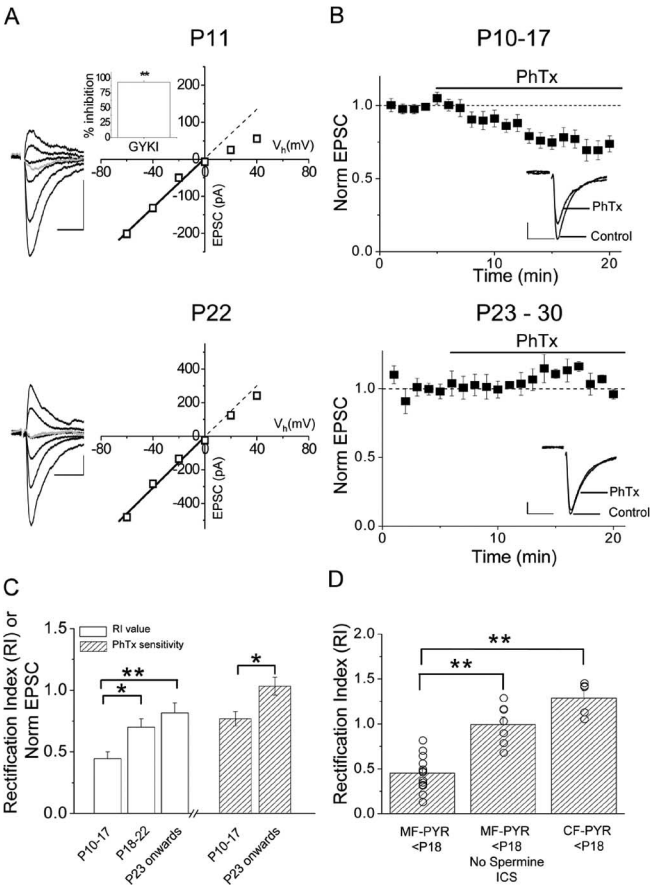

Figure 1. Developmental expression of CP-AMPARs at MF–PYR synapses. ***A***, Representative MF–PYR evoked EPSC *I–V* relationship (V_{hold} from −60 to +40 mV in steps of 20 mV) obtained from a P11 mouse (top panel) and a P22 mouse (bottom panel). Traces are the average of 5–10 events at each holding potential (black). The EPSC at −60 mV after 5 min of DCGIV application to confirm MF origin is indicated in gray. The right panels show plots of the *I–V* relationship: the solid lines represent the linear fit to data points between the −60 and 0 mV holding potentials. The dotted line extends this fit to highlight the deviation of the *I–V* relationship at P11 from linearity. ***B***, Normalized group data show dot plots for the effect of PhTx (2 μM) on evoked MF–PYR EPSCs in slices from mice aged P10–P17 (top panel; $n = 16$) and P23–P30 (bottom panel; $n = 4$). Plotted are the 1 min running average EPSC amplitudes normalized to the average response obtained from the first 5 min of recording before PhTx application. The inset traces are from representative recordings showing average EPSCs (20 events) before (control) and after PhTx treatment (PhTx). ***C***, Summary histogram illustrating the average RI values for, and effects of PhTx on, MF–PYR transmission for the indicated age ranges. PhTx data are expressed as the average EPSC amplitude at the end of PhTx treatment normalized to the average EPSC amplitude obtained immediately preceding PhTx application and are from the recordings in ***B***. RI values were calculated as the ratio of the actual current amplitude at +40 mV to the predicted linear value at +40 mV based on the linear fits of *I–V* relationships illustrated in ***A*** ($n = 13$ for P10–P17; $n = 10$ for P18–P22; and $n = 10$ for P23). ***D***, Bar graph summary comparing the RIs obtained in recordings from P10–P17 mice for MF–PYR synapses ($n = 13$; replotted from ***C***), collateral fiber–PYR synapses ($n = 5$), and for MF–PYR synapses when spermine was omitted from the ICS ($n = 7$). Calibration: 100 pA, 10 ms (throughout the figure). Error bars indicate SEM. Here and throughout, $^*p < 0.05$ and $^{**}p < 0.01$.

SEM, 0.45 ± 0.05; $n = 13$) (Fig. 1*C*,*D*). Importantly, synaptic events were inhibited by >90% during treatment with the AMPAR-specific antagonist GYKI-53655 [1-(4-aminophenyl)-3-methylcarbamyl-4-methyl-7,8-methylenedioxy-3,4-dihydro-5*H*-2,3-benzodiazepine] (40 μM) (Fig. 1*A*, top panel, inset) eliminating the possibility that rectification resulted from KAR (kainate receptor) contamination of EPSCs. It is unlikely that rectification resulted from inadequate voltage clamp of MF–PYR synapses as AMPAR-mediated EPSCs at more distally located collateral fiber–PYR synapses displayed near-linear *I–V* relationships, yielding significantly greater RIs (1.29 ± 0.08; $n = 5$) in slices of comparable age (Fig. 1*D*). Moreover, linear *I–V* relationships with RI values close to unity were obtained in control MF–PYR recordings from young mice using ICS not supplemented with spermine (RI, 0.99 ± 0.08; $n = 7$) (Fig. 1*D*), consistent with a specific role for polyamines in mediating the rectification. The spermine-dependent rectification of EPSCs suggests that CP-AMPARs participate in transmission at developing MF–PYR synapses. Such a contribution of CP-AMPARs to transmission at nascent MF–PYR contacts was subsequently confirmed when we observed partial inhibition of MF–PYR EPSCs by the CP-AMPAR specific antagonist philanthotoxin-433 (PhTx) (2 μM): with 15 min of PhTx perfusion, EPSCs were significantly depressed to 73 ± 4.9% of control ($n = 16$; $p = 0.004$) (Fig. 1*B*, top panel; *C*). Considered together the range of RI values observed and the partial PhTx sensitivity of MF–PYR EPSCs in slices from P10–P17 mice demonstrates that transmission is mediated by a mixed population of both CP- and CI-AMPARs early in development.

Previous investigations did not observe significant rectification (Jonas et al., 1993) or PhTx sensitivity (Toth et al., 2000) of MF–PYR synaptic events in acute rat hippocampal slices. Importantly, this discrepancy with the current findings is not attributable to species differences (Bellone and Luscher, 2005, 2006) because we also observed rectification of MF–PYR EPSCs in acute slices from young (P15–P17) rats (RI, 0.53 ± 0.04; $n = 8$). Although a lack of spermine supplementation may have contributed to the previous failure to observe rectification (Jonas et al., 1993), it is also possible that the contribution of CP-AMPARs at MF–PYR synapses decreases with development as the age range used in the previous studies (P15–P25) was skewed toward animals older than those used in our recordings described above. Indeed, when we examined MF–PYR transmission in slices from older mice (>P17), *I–V* relationships became progressively more linear with increasing age, yielding significantly larger RI values (Fig. 1*A*, bottom, *C*). Similarly, slices from older rats (>P23) yielded significantly greater MF–PYR RIs (0.80 ± 0.06; $n = 7$; $p = 0.006$ vs recordings from P15–P17 rat slices). Furthermore, we did not observe any PhTx sensitivity of MF–PYR synaptic events in slices from older mice (Fig. 1*B*, bottom panel). Thus, the contribution of native CP-AMPARs to MF–PYR transmission is transient, being limited to early developmental time points with subsequent replacement by CI-AMPARs as reported for various other synapses between principal neurons (Aizenman et al., 2002; Kumar et al., 2002; Eybalin et al., 2004).

As an independent test for the participation of CP-AMPARs at developing MF–PYR synapses, we attempted to observe postsynaptic CP-AMPAR-mediated Ca^{2+} transients (CaTs) at MF–PYR contacts in acute hippocampal slices obtained from young (P10–P16) rats (Fig. 2). PYRs were filled with the fluorescent Ca^{2+} indicator OGB-1 through a whole-cell recording electrode and imaged using two-photon laser-scanning microscopy (Fig. 2*A*). After an initial dye loading period (20–30 min), MF–PYR

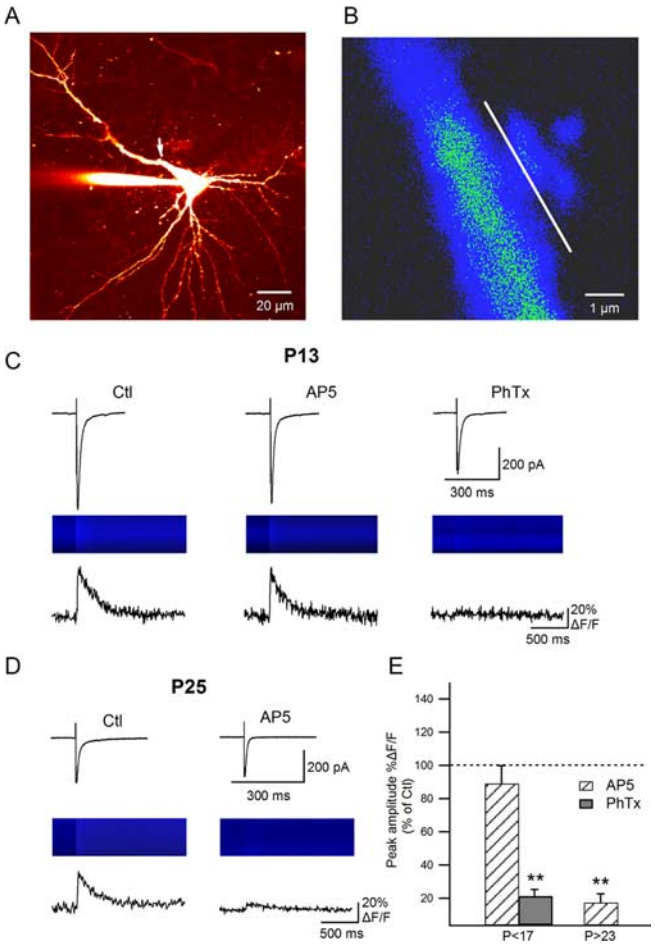

Figure 2. CP-AMPARs mediate CaTs at developing MF–PYR synapses. ***A***, A multiphoton image (*z*-stack) of 60 optical sections taken at 1 μm intervals of an Oregon Green-filled PYR in which MF stimulation evoked CaTs were monitored. ***B***, A pseudocolor image showing basal fluorescence in a thorny excrescence located along the proximal dendrite of the PYR in ***A*** (arrow). The position of the line scan used to monitor stimulus evoked Ca^{2+} signals is indicated parallel to the parent dendrite. ***C***, A representative recording from a P13 rat showing the effects of D-AP5 (50 μM) and PhTx (2 μM) on stimulus evoked CaTs recorded in a thorny excrescence (middle images and bottom traces show raw line scan images and associated CaTs, respectively; average of 4 consecutive events under each condition) and simultaneously monitored EPSCs (top traces; average of 4 consecutive events under each condition). ***D***, Representative recording from a P25 rat showing the effects of AP5 on stimulus evoked CaTs and simultaneously monitored EPSCs. ***E***, Summary histogram for group data examining the effects of AP5 and PhTx on stimulus-evoked CaTs in thorny excrescences from rats aged P10–P16 ($n = 5$) and of AP5 on CaTs in rats older than P23 ($n = 4$). Data are expressed as percentage of control responses that were obtained before any drug treatment. Error bars indicate SEM. $^{**}p < 0.01$, paired *t* test.

postsynaptic elements were identified as large, complex, spine-like protrusions (thorny excrescences) along the proximal apical dendrite (Fig. 2*B*) (Chicurel and Harris, 1992; Reid et al., 2001, 2004). Subsequently, postsynaptic CaTs evoked by local microstimulation within stratum lucidum were monitored within these developing thorny excrescences in line-scanning mode (Fig. 2*B–D*). To maximize the likelihood of observing postsynaptic CaTs, recordings were started with both AMPAR- and NMDAR-mediated transmission intact. Strikingly, in slices from young rats (<P17), MF–PYR CaTs were not significantly affected by NMDAR inhibition but were strongly depressed by subsequent inhibition of CP-AMPARs: CaTs were 89 ± 11% of control after 10 min of D-APV (50 μM) perfusion and further decreased to 21 ± 4% of control after 15 min of PhTx (2 μM) applied with constant synaptic stimulation (0.5Hz) to facilitate use-dependent

block of CP-AMPARs (Fig. 2*C*,*E*). Similarly, simultaneously monitored EPSCs from these recordings were not significantly affected by D-APV (85 ± 7% of control; $p = 0.9$) but exhibited partial sensitivity to PhTx (70 ± 7% of control; $p = 0.04$) (Fig. 2*C*). Although these compound EPSCs represent not only activity at the imaged synapses but also activity at other synapses not under observation, the findings are consistent with those reported above for young mice (compare Fig. 1*B*). In slices from older animals (>P23), MF–PYR CaTs were almost entirely inhibited by D-APV (17 ± 5% of control), indicating that NMDARs are the primary mediators of postsynaptic Ca^{2+} influx at more mature MF–PYR synapses with little or no contribution of CP-AMPARs (Fig. 2*D*,*E*). Together, the results from our imaging experiments confirm that CP-AMPARs transiently participate in transmission greatly contributing to postsynaptic Ca^{2+} dynamics at developing MF–PYR synapses.

CP-AMPARs are preferentially downregulated during MF–PYR DiLTD

In cerebellar stellate cells and dopaminergic neurons of the ventral tegmental area (VTA), CP-AMPARs impart a distinct form of long-term plasticity in which CP-AMPAR-mediated transmission is persistently lost and synapses become dominated by CI-AMPARs (Liu and Cull-Candy, 2000; Bellone and Luscher, 2005; Gardner et al., 2005). In both cases, plasticity is triggered by a rise in postsynaptic Ca^{2+} mediated by influx through the CP-AMPARs themselves or group I mGluR activation during high-frequency stimulation. Recently, we described a novel postsynaptic form of LTD at MF–PYR synapses that is activity independent, being induced simply by transient postsynaptic depolarization (Lei et al., 2003). This DiLTD is expressed as a persistent depression of AMPAR function and, like the plasticities described above, is triggered by a rise in postsynaptic Ca^{2+}, although in this case via influx through L-type voltage-gated Ca^{2+} channels (VGCCs). Importantly, this DiLTD exhibits a developmental profile similar to that observed for the expression of CP-AMPARs at MF–PYR synapses: DiLTD is robust at nascent MF–PYR synapses during the second postnatal week, gradually declines during the third postnatal week, and is absent beyond P35 (Lei et al., 2003). Thus, given the overlapping developmental windows for CP-AMPAR expression and DiLTD competence as well as the role of postsynaptic Ca^{2+} in triggering DiLTD, we next investigated a potential role for modulation of CP-AMPARs in DiLTD.

If MF–PYR DiLTD proceeds as a loss of synaptic CP-AMPARs, similar to CP-AMPAR-associated LTD in the cerebellum and VTA (Liu and Cull-Candy, 2000; Bellone and Luscher, 2005; Gardner et al., 2005), then stimulus evoked synaptic Ca^{2+} influx should be reduced, resulting in a persistent depression of MF–PYR CaTs. Therefore, we initially investigated the effects of DiLTD induction on MF–PYR CaTs in slices from P10–P16 rats (Fig. 3). Synaptic events were evoked at 0.33 Hz and associated CaTs within thorny excrescences were monitored at 1–5 min intervals to minimize potential photodamage. After a stable baseline recording period, presynaptic stimulation was interrupted and the postsynaptic cell was transiently depolarized from a holding potential of −60 to −10 mV for 5 min (Lei et al., 2003) (see Materials and Methods). Subsequently, the postsynaptic membrane potential was returned to −60 mV, presynaptic stimulation was resumed, and the resulting MF–PYR CaTs were recorded for comparison to baseline responses. Using this protocol, we obtained stable CaTs during the baseline recording period; however, immediately after DiLTD induction, a persistent depression of MF–PYR CaTs was evident: CaTs were 36 ± 7.6% of baseline responses immediately after DiLTD induction and ultimately depressed to 6.5 ± 3.4% of baseline responses within 25 min after induction ($n = 5$) (Fig. 3*A*). This LTD of MF–PYR CaTs was paralleled by a persistent inhibition of simultaneously recorded EPSCs (to 73 ± 8.8% of control at 25 min after induction; $p = 0.03$) (Fig. 3*B*). Importantly, in interleaved control recordings, stimulus interruption without concomitant PYR depolarization did not significantly affect MF–PYR CaTs, indicating that CaT LTD did not result from nonspecific rundown of MF–PYR CaTs or photodamage (Fig. 3*A*, inset). Because MF–PYR CaTs measured in thorny excrescences of slices from P10–P16 rats are mediated primarily by CP-AMPARs (Fig. 2), these findings indicate that CP-AMPARs are persistently depressed during DiLTD.

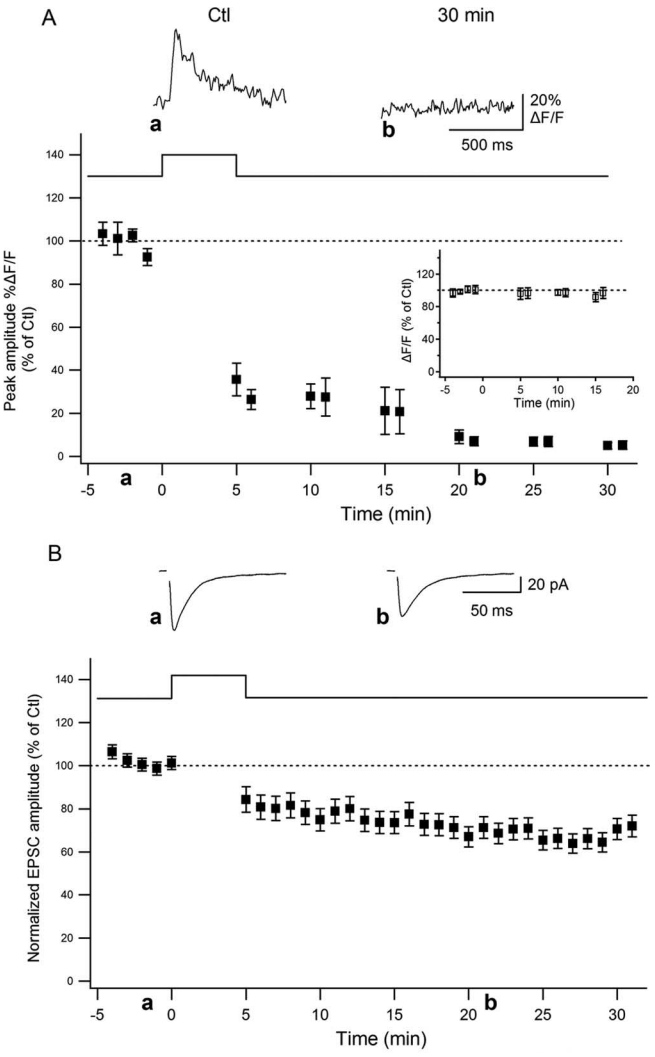

Figure 3. DiLTD results in a loss of postsynaptic MF–PYR CaTs. ***A***, Group data time course plot for experiments in which stimulus evoked CaTs were continuously monitored before and after the DiLTD induction protocol (time, 0 min) was applied ($n = 5$). CaTs (average of 4 events) were monitored at regular intervals during the recordings and expressed as percentage of control CaTs obtained during the baseline recording period. The traces above are CaTs obtained at the times indicated from a representative recording that was subject to the DiLTD induction protocol. The inset time course plot summarizes control recordings in which stimulation was interrupted but PYRs were not subject to depolarization ($n = 3$). ***B***, Group data time course plot showing DiLTD of EPSCs that were recorded during CaT monitoring. EPSC amplitudes for each recording were binned to yield 1 min running averages and are expressed as percentage of control responses obtained during the baseline (preinduction) period. The traces above are EPSCs obtained at the times indicated from the same representative recording that yielded the example CaTs in ***A***. Error bars indicate SEM.

The dramatic depression of MF–PYR CaTs associated with DiLTD is consistent with a long-term inhibition of CP-AMPAR-mediated transmission at MF–PYR synapses allowing transmission to become dominated by CI-AMPARs. If this is the case, then we should be able to detect a DiLTD-induced change in the rectification properties of MF–PYR EPSCs as reported for LTD in cerebellar stellate cells and VTA dopaminergic neurons (Liu and Cull-Candy, 2000, 2005; Bellone and Luscher, 2005; Gardner et al., 2005). Thus, to complement our imaging studies, we next probed for DiLTD-induced changes in RIs of MF–PYR EPSCs. For these experiments, we returned to slices from young mice because we would be examining transgenic animals in later experiments (see below). Moreover, this return to mouse slices allowed us to confirm that the phenomenon of DiLTD, like the expression of CP-AMPARs at MF–PYR synapses, is not species specific. Thus, we first confirmed that mice express DiLTD with properties similar to those observed in rat (Lei et al., 2003). In slices obtained from mice aged P10–P17, transient PYR depolarization from −60 to −10 mV for 5 min produced a depression of MF–PYR EPSCs assayed at −60 mV that persisted for the duration of recordings: 15 min after induction, EPSCs were 63 ± 3.4% of control responses obtained before the depolarization protocol (Fig. 4*A*,*D*). In contrast, transient depolarization did not affect MF–PYR transmission in slices from animals older than P22: EPSCs were 95 ± 17% of control at 15 min after induction (Fig. 4*B*,*D*). As in the rat, DiLTD observed in slices from young mice (P10–P17) did not require synaptic activity during induction and proceeded independent of changes in paired-pulse ratio consistent with postsynaptic induction and expression loci (Fig. 4*A*, inset, bottom panel). Furthermore, loading PYRs with BAPTA significantly inhibited DiLTD in slices from young mice revealing a central role for Ca^{2+} in mouse DiLTD similar to that previously observed in rats (Fig. 4*C*,*D*).

Having confirmed the presence of DiLTD in slices from young mice we proceeded to examine whether rectification of AMPAR-mediated MF–PYR EPSCs is altered by DiLTD by comparing RIs before and after induction (Fig. 5). To avoid potentially confounding influences of the prolonged depolarization periods required to obtain full *I–V* relationships, we adopted an abbreviated RI measure using the absolute value of the ratio of EPSC amplitudes obtained at holding potentials of +40 mV and −60 mV ($RI_{EPSC40/EPSC-60}$) (see Materials and Methods). Importantly, the brief monitoring of EPSCs at +40 mV (average of 5–10 events obtained at 0.33 Hz, thus 15–30 s) during the baseline period did not significantly affect MF–PYR transmission (data not shown), consistent with a minimal 1–3 min depolarization requirement to observe any depression (Lei et al., 2003). In 9 of 10 recordings, we observed that DiLTD produced a greater depression of EPSCs monitored at −60 mV compared with those obtained at +40 mV (Fig. 5*A*). Accordingly, DiLTD was associated with a significant increase in MF–PYR $RI_{EPSC40/EPSC-60}$ values to 157 ± 16% of control at 10 min after induction (Fig. 5*B*). This RI increase indicates that the contribution of inwardly rectifying CP-AMPARs to MF–PYR EPSCs is depressed after DiLTD induction, leaving transmission to be primarily supported by CI-AMPARs.

While monitoring $RI_{EPSC40/EPSC-60}$, we observed that DiLTD is associated with an increase in the PPR for EPSCs monitored at +40 mV, in contrast to events recorded at −60 mV at which no DiLTD-induced change in PPR was detected (Figs. 4*A*, 5*A*, traces). This seemingly contradictory observation likely reflects the inability of spermine blocked CP-AMPARs to contribute to transmission at +40 mV despite the increased release of transmitter on the second pulse of two closely timed stimuli. Indeed the PPR of naive MF–PYR EPSCs measured at +40 mV was significantly less than that obtained at −60 mV with spermine in the recording pipette (1.6 ± 0.12 vs 1.9 ± 0.11 at V_h of +40 and −60, respectively; $n = 10$; $p = 0.04$) (Fig. 5*C*); however, no difference in PPRs at the two holding potentials was evident under spermine-free recording conditions (1.8 ± 0.16 vs 1.7 ± 0.16 at V_h of +40 and −60, respectively; $n = 7$; $p = 0.6$). At naive MF–PYR synapses, use-dependent relief from polyamine block of CP-AMPARs (Rozov et al., 1998; Rozov and Burnashev, 1999; Toth et al., 2000) might be expected to contribute to an increased PPR at +40 mV compared with that at −60 mV (i.e., the larger the degree of initial block the greater opportunity for use-dependent unblock). However, use-dependent unblock does not occur at positive holding potentials between 0 and +60 mV (Ro-

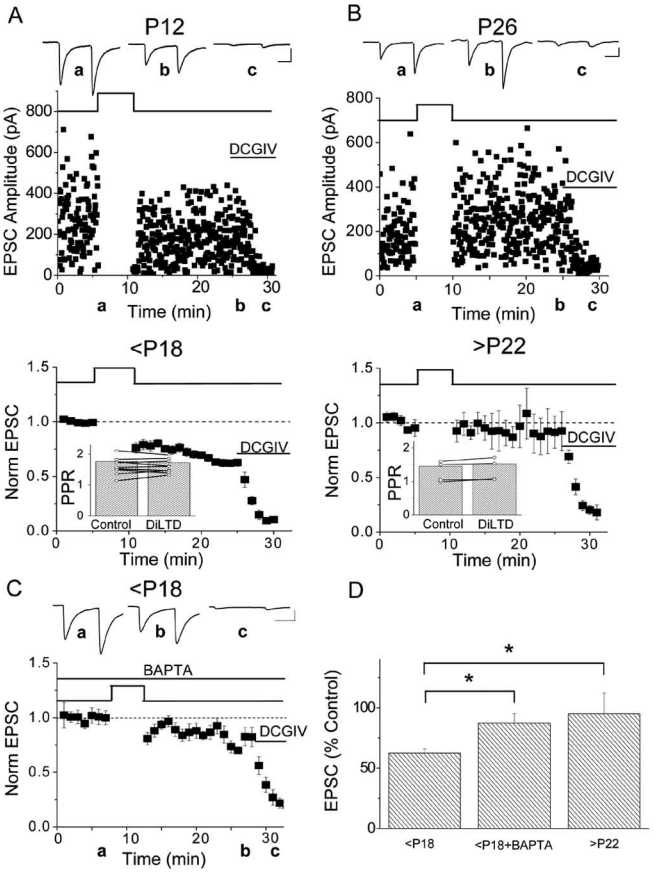

Figure 4. Developmental expression of DiLTD at mouse MF–PYR synapses. ***A***, EPSC amplitude time course plot from a representative recording (top panel) and normalized group data (bottom panel; binned in 1 min intervals and normalized to the first 5 min of recordings) illustrating DiLTD in slices from mice younger than P18 ($n = 26$). The traces above (and throughout the figure) are the average of 20 consecutive EPSC pairs obtained at the times indicated [calbration: 100 pA, 20 ms (throughout the figure)]. Stimulation is paused during induction when the holding potential is moved from −60 to −10 mV for 5 min as indicated. Sensitivity of synaptic events to DCGIV (1 μM) at the end of recordings confirms that inputs are mossy fiber in origin. The inset bar graph in the bottom panel summarizes the PPRs obtained before and after DiLTD induction for a subset of the recordings. ***B***, Similar to ***A***, but for recordings performed in slices from mice older than P22 ($n = 4$). ***C***, Normalized group data for recordings in which the DiLTD induction protocol was attempted in slices from mice younger than P18 with BAPTA (20 mM)-supplemented ICS ($n = 5$). ***D***, Bar graph summary comparing DiLTD for interleaved recordings performed under the conditions indicated. Data are from the recordings making up the group plots in ***A–C*** and represent EPSC amplitudes measured at 15 min after induction expressed as percentage of control responses obtained immediately preceding induction (*$p < 0.05$). Error bars indicate SEM.

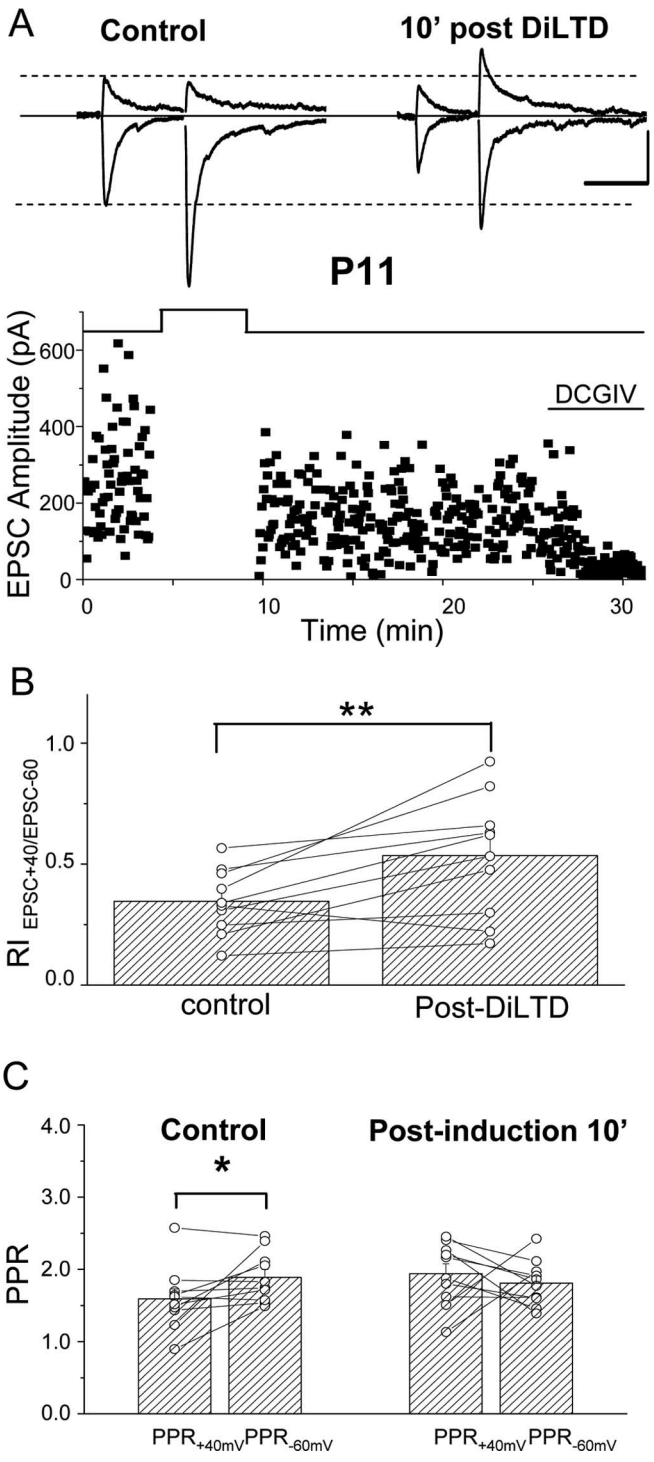

Figure 5. DiLTD reduces rectification of MF–PYR synapses. ***A***, Representative recording in which $RI_{EPSC+40/EPSC-60}$ was monitored before and after DiLTD induction in a slice from a P11 mouse (calibration: 100 pA, 50 ms). The traces above show averaged EPSC pairs evoked at V_h of +40 and −60 mV before DiLTD induction (Control) and 10 min after DiLTD induction (10′ post DiLTD). The bottom panel shows the time course plot of all MF–PYR EPSC amplitudes for this recording before and after DiLTD induction. ***B***, Group data for 10 recordings similar to that illustrated in ***A*** performed in slices from mice aged P10–P17 reveals a significant increase in $RI_{EPSC+40/EPSC-60}$ after DiLTD induction (**$p < 0.01$). Each individual recording is represented by an open circle with the group mean plotted as a bar. ***C***, PPRs measured at holding potentials of +40 and −60 mV before and after DiLTD induction for a subset of the recordings in which $RI_{EPSC+40/EPSC-60}$ was monitored ($n = 8$; *$p < 0.05$). Individual recordings are represented by open circles with group means plotted as bars. Before DiLTD induction the PPR at +40 mV is significantly less than that observed at −60 mV in the same recordings, but after DiLTD the PPRs at +40 and −60 mV are not significantly different.

zov et al., 1998; Rozov and Burnashev, 1999). After DiLTD induction, the increased PPR at +40 mV approximates the PPR observed at −60 mV (Fig. 5*C*) consistent with a switch to transmission being dominated by spermine-insensitive CI-AMPARs. Thus, together, our imaging and electrophysiological data provide compelling evidence for the preferential inhibition of CP-AMPARs during DiLTD at developing MF–PYR synapses, explaining the limited developmental window for this form of synaptic plasticity.

A role for PICK1 in regulating the GluR2 content of MF–PYR synapses

A number of investigations have described a role for the PDZ domain-containing protein PICK1 in regulating the CP-AMPAR content of various central synapses (Terashima et al., 2004; Gardner et al., 2005; Liu and Cull-Candy, 2005; Bellone and Luscher, 2006). Thus, we investigated whether PICK1 participates in controlling the levels of CP-AMPARs at developing MF–PYR synapses.

In cerebellar stellate cells, LTD associated with a loss of CP-AMPAR-mediated transmission is prevented by disruption of PICK1–GluR2 interactions (Gardner et al., 2005; Liu and Cull-Candy, 2005). Because our findings thus far indicate that DiLTD similarly leads to a loss of synaptic CP-AMPARs, we first investigated potential roles for PICK1 in DiLTD using a combination of peptide interference and genetic deletion strategies. Initially, we postsynaptically applied the small interfering peptide EVKI, which selectively disrupts GluR2–PICK1 interactions, through the recording pipette and attempted to induce DiLTD (Daw et al., 2000; Xia et al., 2000; Kim et al., 2001; Gardner et al., 2005; Liu and Cull-Candy, 2005). Because of the variability in time required to find an appropriate MF input after establishing whole-cell configuration, and the close proximity of MF–PYR synapses to the somatic recording location (facilitating rapid dialysis), no effort was made to examine potential peptide influences on transmission during the baseline period. In these recordings, ICS supplemented with the peptide EVKI significantly inhibited DiLTD: 15 min after induction, EPSCs remained at 80 ± 5.7% of control responses ($n = 5$) (Fig. 6*A*,*D*). This inhibition of DiLTD did not result from nonspecific effects of peptide infusion because typical DiLTD was observed in recordings performed with a control peptide SGKA that does not affect PDZ domain-mediated interactions (60 ± 5.3% of control; $n = 5$) (Fig. 6*B*,*D*). Next, we examined DiLTD in slices from young (P10–P17) PICK1 knockout ($PICK1^{-/-}$) mice (Gardner et al., 2005; Steinberg et al., 2006). Consistent with the data from our peptide interference experiments, recordings in slices from $PICK1^{-/-}$ mice revealed a severe deficit in DiLTD: at 15 min after induction, EPSCs were 97 ± 8.6% of control responses ($n = 10$) (Fig. 6*C*,*D*). In contrast, slices from age-matched wild-type ($PICK1^{+/+}$) littermates exhibited robust DiLTD with EPSCs depressing to 63 ± 5.3% of control ($n = 4$) (Fig. 6*D*) comparable with that observed in young C57BL/6 mice used throughout the study to this point (compare Fig. 4*D*).

The blockade of DiLTD by disrupting PICK1 function could be interpreted as evidence for an acute active role of PICK1 in the loss of synaptic CP-AMPARs during DiLTD induction. Alternatively, PICK1 disruption could occlude DiLTD by causing the removal of CP-AMPARs from MF–PYR synapses before induction. Indeed, previous studies have reported alterations in basal synaptic GluR2 content after manipulations of PICK1 function by peptide perfusion or overexpression (Terashima et al., 2004; Gardner et al., 2005). To determine whether EVKI perfusion and

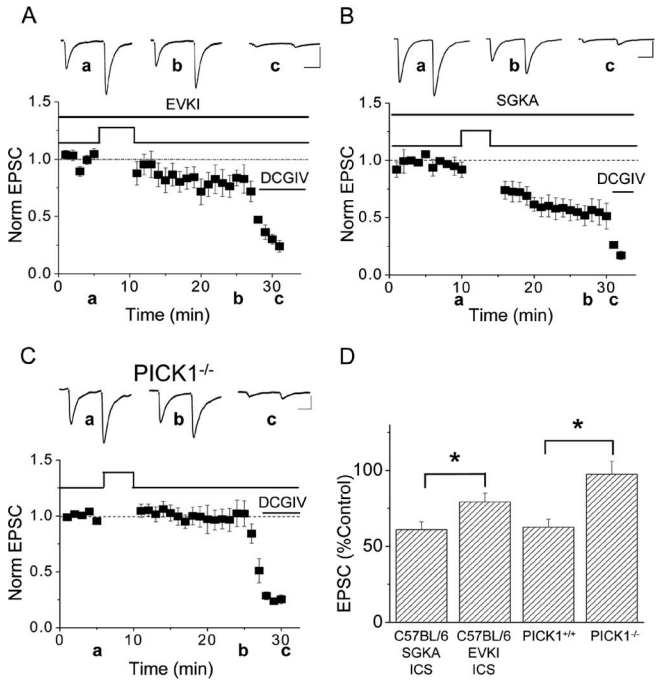

Figure 6. Disruption of PICK1 inhibits DiLTD. ***A***, ***B***, Group data EPSC amplitude time course plots for recordings in which DiLTD induction was attempted in slices from P10–P17 C57BL/6 mice using EVKI-supplemented ICS (***A***; $n = 5$) or SGKA-supplemented ICS (***B***; $n = 5$). The traces above are from representative recordings obtained at the times indicated. ***C***, Group data EPSC amplitude time course plot for recordings in which DiLTD induction was attempted in slices from P10–P17 PICK1 $^{-/-}$ mice ($n = 11$ and 10, 10 and 15 min after induction, respectively). The traces above were obtained during a representative recording at the times indicated. For ***A–C***, EPSC amplitudes were binned as 1 min running averages and normalized to the average EPSC amplitude obtained during the baseline (preinduction) recording period. ***D***, Summary histogram for data presented in ***A–C*** and for recordings performed in P10–P17 PICK1 $^{+/+}$ littermate control mice ($n = 4$). Data represent the EPSC amplitudes at 15 min after induction expressed as a percentage of control responses obtained immediately preceding induction ($^*p < 0.05$). The traces throughout are the average of 20 consecutive events. Calibration: 100 pA, 20 ms. Error bars indicate SEM.

PICK1 knock-out alter the basal contribution of CP-AMPARs to MF–PYR synapses, we examined the rectification properties of MF–PYR EPSCs after peptide treatment and in PICK1 $^{-/-}$ mice. Surprisingly, in slices from young C57BL/6 mice, recordings with EVKI-supplemented ICS yielded MF–PYR EPSCs with near-linear *I–V* relationships resulting in RI values (0.90 ± 0.10; $n = 5$) significantly greater than those obtained with SGKA-supplemented ICS (0.53 ± 0.08; $n = 5$) (Fig. 7*A*,*C*). Similarly, in slices from young PICK1 $^{-/-}$ mice, MF–PYR synapses exhibited RIs significantly greater than those obtained in slices from littermate control PICK1 $^{+/+}$ mice (PICK1 $^{-/-}$: 0.84 ± 0.08, $n = 11$; PICK1 $^{+/+}$: 0.54 ± 0.06, $n = 5$) (Fig. 7*B*,*C*). Furthermore, MF–PYR EPSCs from PICK1 $^{-/-}$ mice were not significantly affected by PhTx treatment (EPSCs were $92 \pm 8.7\%$ of control after 15 min of treatment). Together, these data indicate that loss of PICK1 function acutely by peptide interference, or chronically by genetic ablation, reduces the contribution of CP-AMPARs to developing MF–PYR synapses. Thus, rather than revealing an acute active role for PICK1 in DiLTD, the lack of DiLTD observed in PICK1 $^{-/-}$ mice or after EVKI treatment likely reflects a deficit in the contribution of CP-AMPARs at developing MF–PYR synapses, indicating a critical role for PICK1 in regulating the GluR2 content of developing MF–PYR synapses.

Finally, as an independent assay to probe whether PICK1 regulates the subunit composition of MF–PYR synapses, we performed immunogold electron microscopy (EM) in PYR thorny excrescences of PICK1 $^{+/+}$ and PICK1 $^{-/-}$ mice. Tissue from three different P14 animals for each genotype was double labeled using a polyclonal GluR1-specific antibody and a monoclonal GluR2-specific antibody, and then anti-GluR1 and anti-GluR2 signals were revealed with 5 and 15 nm gold particles, respectively. Consistent with our electrophysiological data, PYR spine profile membranes of PICK1 $^{-/-}$ mice showed a modest reduction in GluR1 signal and a modest increase in GluR2 signal compared with PICK1 $^{+/+}$ littermate controls yielding a significantly larger GluR2/GluR1 signal ratio in PICK1 $^{-/-}$ mice: 0.62 ± 0.1 and 1.0 ± 0.2 for PICK1 $^{+/+}$ and PICK1 $^{-/-}$, respectively ($p = 0.04$) (Fig. 7*D*). Moreover, we observed an increase in the number of synaptic profiles doubly labeled for GluR1 and GluR2 in the absence of PICK1. The ratios of synapses labeled with 5 nm gold particles only, to those labeled with 5 and 15 nm gold particles were 0.98 and 0.64 for PICK1 $^{+/+}$ and PICK1 $^{-/-}$ MF–PYR synapses, respectively (Fig. 7*D*, micrographs) (see Materials and Methods). Thus, considered together, our immuno-EM and electrophysiological data indicate a critical role for PICK1 in the developmental expression of CP-AMPARs at MF–PYR synapses.

Discussion

In the mature CNS, excitatory transmission between principal neurons is dominated by CI-AMPARs because of prominent expression of edited GluR2 subunits within postsynaptic AMPARs. However, GluR2-lacking, CP-AMPARs participate at principal cell synapses early in development in various central structures (Pellegrini-Giampietro et al., 1992; Pickard et al., 2000; Zhu et al., 2000; Aizenman et al., 2002; Kumar et al., 2002; Eybalin et al., 2004; Migues et al., 2007). Here, we examined whether CP-AMPARs contribute at developing MF–PYR synapses using imaging and electrophysiological approaches. We found that MF–PYR transmission within the first 2–3 postnatal weeks uses a mixed population of CP- and CI-AMPARs. CP-AMPAR participation at MF–PYR synapses is developmentally regulated as CI-AMPARs dominate beyond P17. This temporal profile parallels the period during which MF–PYR synapses are DiLTD competent, and our findings suggest that CP-AMPARs are selectively targeted during DiLTD. Consistent with preferential removal of CP-AMPARs during DiLTD, young MF–PYR synapses lacking CP-AMPARs because of PICK1 disruption were DiLTD deficient. These data also revealed that PICK1 regulates the GluR2 content of MF–PYR synapses as reported previously (Terashima et al., 2004; Gardner et al., 2005; Liu and Cull-Candy, 2005; Bellone and Luscher, 2006). We conclude that expression of CP-AMPARs dictates the developmental window for DiLTD and additionally propose that DiLTD proceeds as the PICK1-dependent exchange of CI-AMPARs for CP-AMPARs reminiscent of plasticity in cerebellar stellate cells and VTA neurons (Bellone and Luscher, 2005; Gardner et al., 2005; Liu and Cull-Candy, 2005).

Previous studies did not observe rectifying *I–V* curves or PhTx sensitivity of MF–PYR synaptic events in P15–P25 rat slices (Jonas et al., 1993; Toth et al., 2000). This age range biases toward developmental stages where MF–PYR transmission is entirely supported by CI-AMPARs, likely explaining the differences with our findings. Additionally, Jonas et al. (1993) performed their study before the discovery that CP-AMPAR rectification results from intracellular polyamines, and so it was not common practice to supplement intracellular solutions with polyamines. Because spermine supplementation is critical for MF–PYR rectification (Fig. 1*D*), this may also have contributed to the lack of rectification in the previous investigation. Subsequently, Jonas

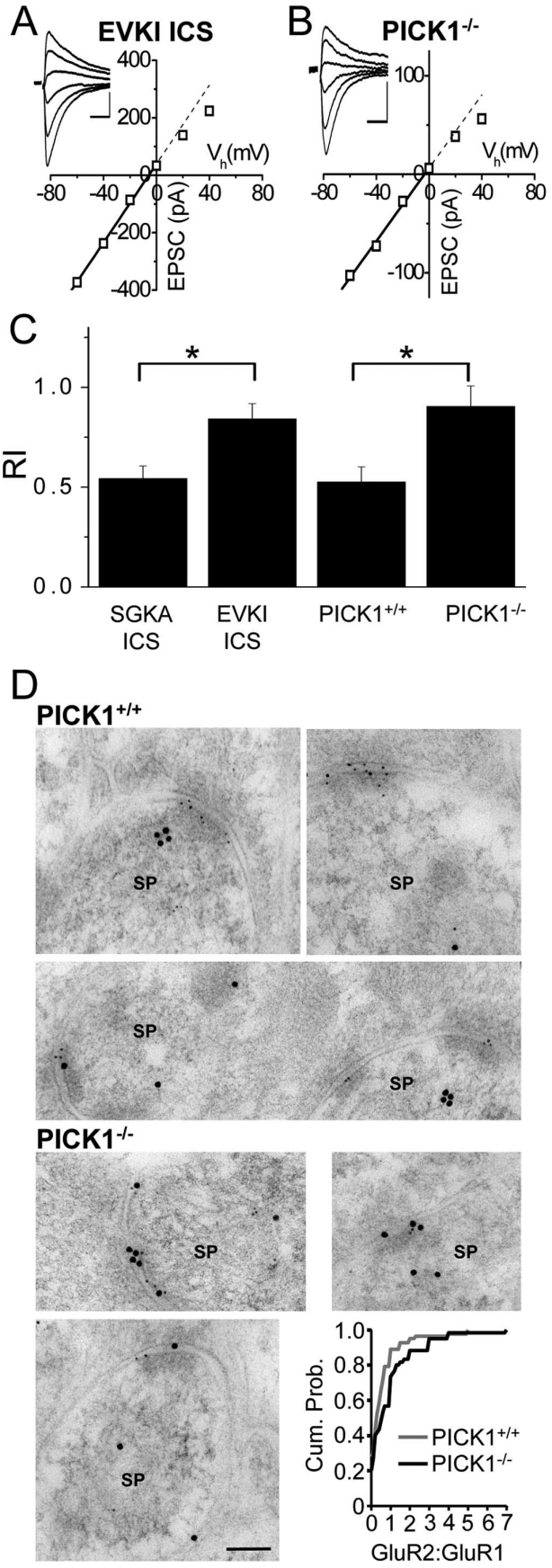

Figure 7. Loss of CP-AMPARs at developing MF–PYR synapses after PICK1 disruption. ***A***, MF–PYR EPSC *I–V* relationship (V_{hold} from −60 to +40 mV in steps of 20 mV) obtained during a representative recording in a slice from a P14 C57BL/6 mouse using EVKI-containing ICS. The line is the linear fit to data points for holding potentials between −60 and 0 mV. The traces are the average of 5–10 events at each holding potential (calibration: 100 pA, 10 ms). ***B***, Representative MF–PYR EPSC *I–V* relationship obtained in a slice from a P14 PICK1 $^{-/-}$ mouse (calibration: 50 pA, 10 ms). ***C***, Group data summary bar chart for RI values obtained in slices from C57BL/6 mice aged P10–P17 using ICS supplemented with EVKI ($n = 5$) or SGKA ($n = 5$). Also shown is the group data summary bar chart of RI values obtained in P10–P17 PICK1 $^{-/-}$ ($n = 11$) and PICK1 $^{+/+}$ ($n = 5$) mice. Error bars indicate SEM. ***D***, Representative photomicrographs of immunogold labeling in PYR spine profiles (SPs) for GluR1 (5 nm gold particle) and GluR2 (15 nm gold particles) in PICK1 $^{+/+}$ mice (top panel; three micrographs showing 4 SPs) and PICK1 $^{-/-}$ mice (bottom left panel; 3 micrographs each with 1 SP). The bottom right panel is a cumulative probability histogram (bin width, 0.1) of GluR2/GluR1 signal ratios in SP membranes of PICK1 $^{+/+}$ mice ($n = 87$ SPs from 3 animals) and PICK1 $^{-/-}$ mice ($n = 66$ SPs from 3 animals). Scale bar (bottom left photomicrograph), 100 nm. *$p < 0.05$ throughout the figure.

and colleagues examined rectification properties of PYR somatic membrane patches from P13–P15 rat slices and again observed linear *I–V* relationships even with spermine present (Koh et al., 1995). This difference with our findings cannot be attributed to age differences or lack of spermine supplementation and, thus, indicates that young PYR extrasynaptic membranes are rich in CI-AMPARs. Similarly, CI-AMPARs dominate extrasynaptic membranes of cerebellar stellate cells and developing layer 5 pyramids despite synaptic expression of CP-AMPARs (Liu and Cull-Candy, 2000, 2002; Kumar and Huguenard, 2001; Kumar et al., 2002; Gardner et al., 2005). We additionally found that associational/commissural-PYR transmission is mediated solely by CI-AMPARs during early development. Considered together, the evidence indicates that during the first 2–3 postnatal weeks PYRs express CP-AMPARs in a synapse-specific manner.

Species-dependent differences in synaptic expression of CP-AMPARs also exist (Bellone and Luscher, 2005, 2006); therefore, we considered whether our observations in mouse differed from previous reports because of choice of experimental animal. However, both imaging and electrophysiological recordings confirmed participation of CP-AMPARs at developing rat MF–PYR synapses. Our imaging experiments also provided direct evidence for Ca^{2+} permeability of MF–PYR AMPARs, an important consideration because Ca^{2+} permeability is more sensitive to GluR2 content than is rectification or PhTx sensitivity (Dingledine et al., 1992; Washburn et al., 1997). A previous study in slice culture found that MF evoked CaTs in PYR spines were insensitive to the CP-AMPAR antagonist HPP-spermine [*N*-(4-hydroxyphenylpropanoyl)-spermine] (Reid et al., 2001). Again, this discrepancy with our findings likely reflects the limited developmental expression of CP-AMPARs at MF–PYR synapses as slices were obtained at P8 and cultured for 10–21 d.

CP-AMPARs impart distinct short- and long-term plasticity to various central synapses (Rozov et al., 1998; Rozov and Burnashev, 1999; Liu and Cull-Candy, 2000; Toth et al., 2000; Lei and McBain, 2002; Bellone and Luscher, 2005; Gardner et al., 2005; Pelkey et al., 2005, 2006; Shin et al., 2005). The loss of CaTs and decreased rectification after DiLTD induction indicate that CP-AMPARs are selectively depressed during DiLTD. Accordingly, MF–PYR synapses devoid of CP-AMPARs, in slices from older animals or after PICK1 disruption, do not exhibit DiLTD. The CI-AMPARs that support transmission after DiLTD appear to principally reflect the population initially present at naive synapses. However, the occasionally observed EPSC growth at +40 mV, particularly for the second EPSC in pairs of events (Fig. 5*A*, traces), suggests that CI-AMPARs may also be exchanged for CP-AMPARs after DiLTD, similar to LTD in cerebellar stellate cells and dopaminergic VTA neurons (Liu and Cull-Candy, 2000;

Bellone and Luscher, 2005; Gardner et al., 2005). The initial wide range of RIs at naive MF–PYR synapses combined with the large variability in presynaptic release and low number of events collected at +40 mV in the recordings may have confounded reliable detection of EPSC growth at positive potentials. The greater success in observing such growth on the second EPSC of evoked pairs could reflect increased release probability combined with perisynaptic localization of new CI-AMPARs that will diffuse laterally to postsynaptic sites.

The critical trigger for DiLTD induction is an increase in postsynaptic Ca^{2+} by influx through L-type VGCCs and release from intracellular stores (Lei et al., 2003). Similarly, loss of synaptic CP-AMPARs in cerebellar stellate cells and VTA dopaminergic neurons is triggered by increased intracellular Ca^{2+} (Liu and Cull-Candy, 2000; Bellone and Luscher, 2005). CP-AMPAR removal may serve a protective feedback mechanism to combat additional cytosolic Ca^{2+} increases that can be deleterious for the postsynaptic cell (Sattler and Tymianski, 2000; Arundine and Tymianski, 2003). The physiological trigger for the developmental loss of CP-AMPARs at MF–PYR synapses remains unknown. However, PYRs exhibit intense burst firing early in development and such firing could effectively activate L-type VGCCs, expression of which is upregulated between P8 and P21 and localizes to proximal dendrites near MF inputs (Westenbroek et al., 1990; Glazewski et al., 1993; Hell et al., 1993; Elliott et al., 1995). Alternatively, excess Ca^{2+} influx through the CP-AMPARs themselves could provide a self-regulating mechanism triggering CP-AMPARs removal (Liu and Cull-Candy, 2000).

The loss of CP-AMPAR-mediated MF–PYR transmission after PICK1 disruption was surprising because cerebellar stellate cells maintain, or even increase, the synaptic complement of CP-AMPARs after EVKI treatment or PICK1 knock-out (Gardner et al., 2005; Liu and Cull-Candy, 2005). However, our findings are consistent with observations in CA1 pyramids in which PICK1 overexpression promotes CP-AMPAR accumulation at synapses, whereas EVKI overexpression increases GluR2 content (Terashima et al., 2004). Similarly, small interfering RNA knockdown of PICK1 promotes membrane insertion of GluR2-containing receptors (Sossa et al., 2006). Development of a unified model for PICK1 in regulating synaptic AMPAR composition is hampered by conflicting findings at distinct synapses, suggesting that PICK1 functions in a cell- and synapse-specific manner. For example, a well defined role for PICK1 in GluR2-containing AMPAR internalization exists at cerebellar parallel fiber–Purkinje neuron synapses (Xia et al., 2000; Steinberg et al., 2006), whereas stellate cells require PICK1 for synaptic delivery of GluR2-containing AMPARs (Gardner et al., 2005; Liu and Cull-Candy, 2005). Thus, evidence supports roles for PICK1 in AMPAR internalization and surface delivery. Indeed, PICK1 supports bidirectional changes in surface AMPARs (Sossa et al., 2006). This duality of function likely reflects the Ca^{2+} binding properties of PICK1, which yield bimodal regulation of PICK1–GluR2 interactions (Hanley and Henley, 2005; Sossa et al., 2006). Our findings suggest a model in which PICK1 maintains intracellular pools of GluR2-containing AMPARs (Jin et al., 2006), which are trafficked to the surface after appropriate stimuli like increased intracellular Ca^{2+}. Loss of PICK1–GluR2 interactions by highly elevated intracellular Ca^{2+}, EVKI treatment, or PICK1 knock-out could promote mobilization of this CI-AMPAR intracellular pool to the surface, which subsequently may trigger removal of synaptic CP-AMPARs, allowing for synaptic incorporation of the CI-AMPARs through lateral diffusion. Although additional investigation is needed to characterize molecular events controlling AMPAR trafficking at MF–PYR synapses, our findings further implicate PICK1 as an important regulator of synaptic GluR2 (Terashima et al., 2004; Bellone and Luscher, 2005; Gardner et al., 2005; Liu and Cull-Candy, 2005).

In conclusion, we found that CP-AMPARs contribute to nascent MF–PYR transmission within the first 3 postnatal weeks. This early participation of CP-AMPARs may provide a postsynaptic Ca^{2+} signal important for synapse maturation. Developing synapses are believed to proceed from silent, with transmission solely mediated by NMDARs, to functional by the stepwise acquisition of AMPARs (Isaac, 2003; Poncer, 2003). Our findings along with other reports (Pellegrini-Giampietro et al., 1992; Pickard et al., 2000; Zhu et al., 2000; Aizenman et al., 2002; Kumar et al., 2002; Eybalin et al., 2004; Migues et al., 2007) indicate the transient incorporation of CP-AMPARs may represent a previously unappreciated step at many central synapses in this model. Interestingly, a similar phenomenon may occur during various forms of synaptic plasticity in the mature CNS, although on more rapid timescales (Thiagarajan et al., 2005; Clem and Barth, 2006; McCormack et al., 2006; Plant et al., 2006; Sutton et al., 2006), further linking the processes of synapse development and plasticity.

References

Aizenman CD, Munoz-Elias G, Cline HT (2002) Visually driven modulation of glutamatergic synaptic transmission is mediated by the regulation of intracellular polyamines. Neuron 34:623–634.

Amaral DG, Dent JA (1981) Development of the mossy fibers of the dentate gyrus: I. A light and electron microscopic study of the mossy fibers and their expansions. J Comp Neurol 195:51–86.

Arundine M, Tymianski M (2003) Molecular mechanisms of calcium-dependent neurodegeneration in excitotoxicity. Cell Calcium 34:325–337.

Bagal AA, Kao JP, Tang CM, Thompson SM (2005) Long-term potentiation of exogenous glutamate responses at single dendritic spines. Proc Natl Acad Sci USA 102:14434–14439.

Bellone C, Luscher C (2005) mGluRs induce a long-term depression in the ventral tegmental area that involves a switch of the subunit composition of AMPA receptors. Eur J Neurosci 21:1280–1288.

Bellone C, Luscher C (2006) Cocaine triggered AMPA receptor redistribution is reversed in vivo by mGluR-dependent long-term depression. Nat Neurosci 9:636–641.

Bowie D, Mayer ML (1995) Inward rectification of both AMPA and kainate subtype glutamate receptors generated by polyamine-mediated ion channel block. Neuron 15:453–462.

Burnashev N, Monyer H, Seeburg PH, Sakmann B (1992) Divalent ion permeability of AMPA receptor channels is dominated by the edited form of a single subunit. Neuron 8:189–198.

Chicurel ME, Harris KM (1992) Three-dimensional analysis of the structure and composition of CA3 branched dendritic spines and their synaptic relationships with mossy fiber boutons in the rat hippocampus. J Comp Neurol 325:169–182.

Clem RL, Barth A (2006) Pathway-specific trafficking of native AMPARs by in vivo experience. Neuron 49:663–670.

Collingridge GL, Isaac JT, Wang YT (2004) Receptor trafficking and synaptic plasticity. Nat Rev Neurosci 5:952–962.

Darstein M, Petralia RS, Swanson GT, Wenthold RJ, Heinemann SF (2003) Distribution of kainate receptor subunits at hippocampal mossy fiber synapses. J Neurosci 23:8013–8019.

Daw MI, Chittajallu R, Bortolotto ZA, Dev KK, Duprat F, Henley JM, Collingridge GL, Isaac JT (2000) PDZ proteins interacting with C-terminal GluR2/3 are involved in a PKC-dependent regulation of AMPA receptors at hippocampal synapses. Neuron 28:873–886.

Dingledine R, Hume RI, Heinemann SF (1992) Structural determinants of barium permeation and rectification in non-NMDA glutamate receptor channels. J Neurosci 12:4080–4087.

Dingledine R, Borges K, Bowie D, Traynelis SF (1999) The glutamate receptor ion channels. Pharmacol Rev 51:7–61.

Donevan SD, Rogawski MA (1995) Intracellular polyamines mediate in-

ward rectification of Ca^{2+}-permeable alpha-amino-3-hydroxy-5-methyl-4-isoxazolepropionic acid receptors. Proc Natl Acad Sci USA 92:9298–9302.

Elliott EM, Malouf AT, Catterall WA (1995) Role of calcium channel subtypes in calcium transients in hippocampal CA3 neurons. J Neurosci 15:6433–6444.

Eybalin M, Caicedo A, Renard N, Ruel J, Puel JL (2004) Transient Ca^{2+}-permeable AMPA receptors in postnatal rat primary auditory neurons. Eur J Neurosci 20:2981–2989.

Gardner SM, Takamiya K, Xia J, Suh JG, Johnson R, Yu S, Huganir RL (2005) Calcium-permeable AMPA receptor plasticity is mediated by subunit-specific interactions with PICK1 and NSF. Neuron 45:903–915.

Glazewski S, Skangiel-Kramska J, Kossut M (1993) Development of NMDA receptor-channel complex and L-type calcium channels in mouse hippocampus. J Neurosci Res 35:199–206.

Hanley JG, Henley JM (2005) PICK1 is a calcium-sensor for NMDA-induced AMPA receptor trafficking. EMBO J 24:3266–3278.

Harms KJ, Tovar KR, Craig AM (2005) Synapse-specific regulation of AMPA receptor subunit composition by activity. J Neurosci 25:6379–6388.

Hell JW, Westenbroek RE, Warner C, Ahlijanian MK, Prystay W, Gilbert MM, Snutch TP, Catterall WA (1993) Identification and differential subcellular localization of the neuronal class C and class D L-type calcium channel alpha 1 subunits. J Cell Biol 123:949–962.

Henze DA, Urban NN, Barrionuevo G (2000) The multifarious hippocampal mossy fiber pathway: a review. Neuroscience 98:407–427.

Hollmann M, Hartley M, Heinemann S (1991) Ca^{2+} permeability of KA-AMPA–gated glutamate receptor channels depends on subunit composition. Science 252:851–853.

Isaac JT (2003) Postsynaptic silent synapses: evidence and mechanisms. Neuropharmacology 45:450–460.

Isaac JT, Ashby M, McBain CJ (2007) The role of the GluR2 subunit in AMPA receptor function and synaptic plasticity. Neuron 54:859–871.

Jin W, Ge WP, Xu J, Cao M, Peng L, Yung W, Liao D, Duan S, Zhang M, Xia J (2006) Lipid binding regulates synaptic targeting of PICK1, AMPA receptor trafficking, and synaptic plasticity. J Neurosci 26:2380–2390.

Jonas P, Major G, Sakmann B (1993) Quantal components of unitary EPSCs at the mossy fibre synapse on CA3 pyramidal cells of rat hippocampus. J Physiol (Lond) 472:615–663.

Ju W, Morishita W, Tsui J, Gaietta G, Deerinck TJ, Adams SR, Garner CC, Tsien RY, Ellisman MH, Malenka RC (2004) Activity-dependent regulation of dendritic synthesis and trafficking of AMPA receptors. Nat Neurosci 7:244–253.

Kakegawa W, Tsuzuki K, Yoshida Y, Kameyama K, Ozawa S (2004) Input- and subunit-specific AMPA receptor trafficking underlying long-term potentiation at hippocampal CA3 synapses. Eur J Neurosci 20:101–110.

Kamboj SK, Swanson GT, Cull-Candy SG (1995) Intracellular spermine confers rectification on rat calcium-permeable AMPA and kainate receptors. J Physiol (Lond) 486:297–303.

Kamiya H, Shinozaki H, Yamamoto C (1996) Activation of metabotropic glutamate receptor type 2/3 suppresses transmission at rat hippocampal mossy fibre synapses. J Physiol (Lond) 493:447–455.

Kim CH, Chung HJ, Lee HK, Huganir RL (2001) Interaction of the AMPA receptor subunit GluR2/3 with PDZ domains regulates hippocampal long-term depression. Proc Natl Acad Sci USA 98:11725–11730.

Koh DS, Burnashev N, Jonas P (1995) Block of native $Ca(^{2+})$-permeable AMPA receptors in rat brain by intracellular polyamines generates double rectification. J Physiol (Lond) 486:305–312.

Kumar SS, Huguenard JR (2001) Properties of excitatory synaptic connections mediated by the corpus callosum in the developing rat neocortex. J Neurophysiol 86:2973–2985.

Kumar SS, Bacci A, Kharazia V, Huguenard JR (2002) A developmental switch of AMPA receptor subunits in neocortical pyramidal neurons. J Neurosci 22:3005–3015.

Lei S, McBain CJ (2002) Distinct NMDA receptors provide differential modes of transmission at mossy fiber-interneuron synapses. Neuron 33:921–933.

Lei S, Pelkey KA, Topolnik L, Congar P, Lacaille JC, McBain CJ (2003) Depolarization-induced long-term depression at hippocampal mossy fiber-CA3 pyramidal neuron synapses. J Neurosci 23:9786–9795.

Liu SJ, Cull-Candy SG (2002) Activity-dependent change in AMPA receptor properties in cerebellar stellate cells. J Neurosci 22:3881–3889.

Liu SJ, Cull-Candy SG (2005) Subunit interaction with PICK and GRIP controls Ca^{2+} permeability of AMPARs at cerebellar synapses. Nat Neurosci 8:768–775.

Liu SQ, Cull-Candy SG (2000) Synaptic activity at calcium-permeable AMPA receptors induces a switch in receptor subtype. Nature 405:454–458.

McCormack SG, Stornetta RL, Zhu JJ (2006) Synaptic AMPA receptor exchange maintains bidirectional plasticity. Neuron 50:75–88.

Migues PV, Cammarota M, Kavanagh J, Atkinson R, Powis DA, Rostas JA (2007) Maturational changes in the subunit composition of AMPA receptors and the functional consequences of their activation in chicken forebrain. Dev Neurosci 29:232–240.

Ogoshi F, Yin HZ, Kuppumbatti Y, Song B, Amindari S, Weiss JH (2005) Tumor necrosis-factor-alpha (TNF-alpha) induces rapid insertion of Ca^{2+}-permeable alpha-amino-3-hydroxyl-5-methyl-4-isoxazolepropionate (AMPA)/kainate (Ca-A/K) channels in a subset of hippocampal pyramidal neurons. Exp Neurol 193:384–393.

Pelkey KA, Lavezzari G, Racca C, Roche KW, McBain CJ (2005) mGluR7 is a metaplastic switch controlling bidirectional plasticity of feedforward inhibition. Neuron 46:89–102.

Pelkey KA, Topolnik L, Lacaille JC, McBain CJ (2006) Compartmentalized Ca^{2+} channel regulation at divergent mossy-fiber release sites underlies target cell-dependent plasticity. Neuron 52:497–510.

Pellegrini-Giampietro DE, Zukin RS, Bennett MV, Cho S, Pulsinelli WA (1992) Switch in glutamate receptor subunit gene expression in CA1 subfield of hippocampus following global ischemia in rats. Proc Natl Acad Sci USA 89:10499–10503.

Petralia RS, Wenthold RJ (1992) Light and electron immunocytochemical localization of AMPA-selective glutamate receptors in the rat brain. J Comp Neurol 318:329–354.

Petralia RS, Wenthold RJ (1999) Immunocytochemistry of NMDA receptors. Methods Mol Biol 128:73–92.

Petralia RS, Esteban JA, Wang YX, Partridge JG, Zhao HM, Wenthold RJ, Malinow R (1999) Selective acquisition of AMPA receptors over postnatal development suggests a molecular basis for silent synapses. Nat Neurosci 2:31–36.

Pickard L, Noel J, Henley JM, Collingridge GL, Molnar E (2000) Developmental changes in synaptic AMPA and NMDA receptor distribution and AMPA receptor subunit composition in living hippocampal neurons. J Neurosci 20:7922–7931.

Plant K, Pelkey KA, Bortolotto ZA, Morita D, Terashima A, McBain CJ, Collingridge GL, Isaac JT (2006) Transient incorporation of native GluR2-lacking AMPA receptors during hippocampal long-term potentiation. Nat Neurosci 9:602–604.

Poncer JC (2003) Hippocampal long term potentiation: silent synapses and beyond. J Physiol (Paris) 97:415–422.

Reid CA, Fabian-Fine R, Fine A (2001) Postsynaptic calcium transients evoked by activation of individual hippocampal mossy fiber synapses. J Neurosci 21:2206–2214.

Reid CA, Dixon DB, Takahashi M, Bliss TV, Fine A (2004) Optical quantal analysis indicates that long-term potentiation at single hippocampal mossy fiber synapses is expressed through increased release probability, recruitment of new release sites, and activation of silent synapses. J Neurosci 24:3618–3626.

Rouach N, Byrd K, Petralia RS, Elias GM, Adesnik H, Tomita S, Karimzadegan S, Kealey C, Bredt DS, Nicoll RA (2005) TARP gamma-8 controls hippocampal AMPA receptor number, distribution and synaptic plasticity. Nat Neurosci 8:1525–1533.

Rozov A, Burnashev N (1999) Polyamine-dependent facilitation of postsynaptic AMPA receptors counteracts paired-pulse depression. Nature 401:594–598.

Rozov A, Zilberter Y, Wollmuth LP, Burnashev N (1998) Facilitation of currents through rat Ca^{2+}-permeable AMPA receptor channels by activity-dependent relief from polyamine block. J Physiol (Lond) 511:361–377.

Sattler R, Tymianski M (2000) Molecular mechanisms of calcium-dependent excitotoxicity. J Mol Med 78:3–13.

Seeburg PH, Higuchi M, Sprengel R (1998) RNA editing of brain glutamate receptor channels: mechanism and physiology. Brain Res Brain Res Rev 26:217–229.

Shin J, Shen F, Huguenard JR (2005) Polyamines modulate AMPA

receptor-dependent synaptic responses in immature layer v pyramidal neurons. J Neurophysiol 93:2634–2643.

Sommer B, Kohler M, Sprengel R, Seeburg PH (1991) RNA editing in brain controls a determinant of ion flow in glutamate-gated channels. Cell 67:11–19.

Sossa KG, Court BL, Carroll RC (2006) NMDA receptors mediate calcium-dependent, bidirectional changes in dendritic PICK1 clustering. Mol Cell Neurosci 31:574–585.

Steinberg JP, Takamiya K, Shen Y, Xia J, Rubio ME, Yu S, Jin W, Thomas GM, Linden DJ, Huganir RL (2006) Targeted in vivo mutations of the AMPA receptor subunit GluR2 and its interacting protein PICK1 eliminate cerebellar long-term depression. Neuron 49:845–860.

Sutton MA, Ito HT, Cressy P, Kempf C, Woo JC, Schuman EM (2006) Miniature neurotransmission stabilizes synaptic function via tonic suppression of local dendritic protein synthesis. Cell 125:785–799.

Terashima A, Cotton L, Dev KK, Meyer G, Zaman S, Duprat F, Henley JM, Collingridge GL, Isaac JT (2004) Regulation of synaptic strength and AMPA receptor subunit composition by PICK1. J Neurosci 24:5381–5390.

Thiagarajan TC, Lindskog M, Tsien RW (2005) Adaptation to synaptic inactivity in hippocampal neurons. Neuron 47:725–737.

Topolnik L, Congar P, Lacaille JC (2005) Differential regulation of metabotropic glutamate receptor- and AMPA receptor-mediated dendritic Ca^{2+} signals by presynaptic and postsynaptic activity in hippocampal interneurons. J Neurosci 25:990–1001.

Toth K, Suares G, Lawrence JJ, Philips-Tansey E, McBain CJ (2000) Differential mechanisms of transmission at three types of mossy fiber synapse. J Neurosci 20:8279–8289.

Verdoorn TA, Burnashev N, Monyer H, Seeburg PH, Sakmann B (1991) Structural determinants of ion flow through recombinant glutamate receptor channels. Science 252:1715–1718.

Washburn MS, Numberger M, Zhang S, Dingledine R (1997) Differential dependence on GluR2 expression of three characteristic features of AMPA receptors. J Neurosci 17:9393–9406.

Westenbroek RE, Ahlijanian MK, Catterall WA (1990) Clustering of L-type Ca^{2+} channels at the base of major dendrites in hippocampal pyramidal neurons. Nature 347:281–284.

Xia J, Chung HJ, Wihler C, Huganir RL, Linden DJ (2000) Cerebellar long-term depression requires PKC-regulated interactions between GluR2/3 and PDZ domain-containing proteins. Neuron 28:499–510.

Zhu JJ, Esteban JA, Hayashi Y, Malinow R (2000) Postnatal synaptic potentiation: delivery of GluR4-containing AMPA receptors by spontaneous activity. Nat Neurosci 3:1098–1106.